Three-Dimensional Solution Structure of the N-Terminal Domain of DNA Polymerase β and Mapping of the ssDNA Interaction Interface[†,‡]

Dingjiang Liu,[§,||] Rajendra Prasad,[⊥] Samuel H. Wilson,[⊥] Eugene F. DeRose,[#] and Gregory P. Mullen*[,§]

Department of Biochemistry, University of Connecticut Health Center, Farmington, Connecticut 06032, Sealy Center for Molecular Science, The University of Texas Medical Branch, Galveston, Texas 77555, and Department of Chemistry, University of Wisconsin−Milwaukee, Milwaukee, Wisconsin 53201

Received November 7, 1995; Revised Manuscript Received February 21, 1996[⊗]

ABSTRACT: DNA polymerase β (β-Pol) consists of an N-terminal ssDNA binding domain with deoxyribose phosphodiesterase activity and a C-terminal domain with nucleotidyltransferase activity. The solution structure of the cloned N-terminal domain of β-Pol has been determined by multidimensional heteronuclear NMR using experimental restraints that included 1030 distances based on analysis of NOE connectivities, 68 ϕ, χ_1, and χ_2 torsion angles based on analysis of couplings, and 22 hydrogen bonds. Hydrogen bonds were assessed only within helices by the absence of saturation transfer from water at pH 6.7, by NOEs and $J_{NH\alpha}$ couplings indicative of well-structured helices, and by $^{13}C_\alpha$ chemical shifts characteristic of helices. The root mean square deviation for heavy backbone atoms within the helices was 0.64 Å in 55 structures. The solution structure of the N-terminal domain is formed from four helices packed as two antiparallel pairs crossing at 50° in a V-like shape. The domain binds $p(dT)_8$, a template analogue, as a 1:1 complex in 100 mM NaCl (K_D = 10 μM). Analysis of the binding equilibria at increasing NaCl concentrations indicated that ionic contacts contribute to the complex. The binding interaction was mapped to one face of the domain by characterizing backbone ^1H and ^{15}N chemical shift changes. Assigned intermolecular NOEs from 2D NOESY support the assessment of the binding interface. The structure that forms the interaction surface includes an antiparallel helix-3−turn−helix-4 motif and residues adjacent to an Ω-type loop connecting helix-1 and helix-2. Sites appropriate for nucleotide contact on the structure are described. The mapped interaction interface for a ssDNA template is the first described for a DNA polymerase.

β-Pol[1] catalyzes DNA synthesis using a template-primer or a gapped DNA substrate, deoxynucleoside triphosphates, and Mg^{2+} in the penultimate step of short-patch DNA repair. β-Pol is a required DNA polymerase in a reconstituted base excision repair system and is the only mammalian polymerase displaying DNA synthesis activity with DNA substrates containing G-U mismatches (Singhal et al., 1995). Gap binding is strongly dependent on the presence of a 5′-phosphate on a downstream primer. Unlike other mammalian polymerases, β-Pol fills the DNA gap to completion (Singhal & Wilson, 1993; Prasad et al., 1994). The high frequency of misincorporations catalyzed by β-Pol is unusual for DNA polymerases in mammals. On average the enzyme inserts 1 incorrect nucleotide for every 5000 nucleotides polymerized on a singly primed M13 template (Kunkel, 1985), catalyzes misincorporation via template misalignment (Boosalis et al., 1989), and extends primer-template mismatches (Shibutani et al., 1993).

DNA polymerase β is the smallest known DNA polymerase in animal cells (M_r 39 000) (Fry & Loeb, 1986) and is highly conserved among mammals. Characterization of the NMR solution structure has been directed toward the N-terminal and catalytic domains of the enzyme (Liu et al., 1994; Mullen, 1995). β-Pol displays sequence homology to the terminal deoxynucleotidyltransferase within both the catalytic domain and the N-terminal ssDNA binding domains (Anderson et al., 1987). β-Pol is not homologous to other DNA polymerases. The proteolytically cleavable ssDNA binding N-terminal domain (residues 1−87) of β-Pol has been found by UV light cross-linking to bind in proximity to the upstream, downstream, and template DNA strands in a five-nucleotide gap (Prasad et al., 1994). Using the purified recombinant N-terminal domain, photochemical cross-linking studies showed that residues S30 and H34 cross-linked to $p(dT)_{16}$ (Prasad et al., 1993). The N-terminal domain constitutes ∼25% of the β-Pol primary structure and

[†] This research was supported by Grants GM52738 (G.P.M.) and ES06839 and ES06676 (S.H.W.) from the National Institutes of Health and Grant H-1265 (S.H.W.) from the Welch Foundation.

[‡] Restraints files, coordinates, and individual energies for the superimposed 55 SA structures and the minimized average structure have been deposited in the Brookhaven Protein Data Bank under the accession codes 1bnp and 1bno, respectively.

* To whom correspondence should be addressed. Tel. (860) 679-1943; Fax (860) 679-3408; Email gmullen@panda.uchc.edu.

[§] University of Connecticut Health Center.

[||] Present address: Department of Medical Biophysics, University of Toronto.

[⊥] University of Texas Medical Branch.

[#] University of Wisconsin−Milwaukee.

[⊗] Abstract published in *Advance ACS Abstracts,* May 1, 1996.

[1] Abbreviations: β-Pol, DNA polymerase β; dRPase, deoxyribose phosphodiesterase; NMR, nuclear magnetic resonance; 1D, one dimensional; 2D, two dimensional; 3D, three dimensional; DQF-COSY, double-quantum-filtered correlated spectroscopy; TOCSY, total correlation spectroscopy; NOESY, nuclear Overhauser effect spectroscopy; HMQC, heteronuclear multiple-quantum correlated spectroscopy; HMQC-J, heteronuclear multiple-quantum *J*-resolved spectroscopy; HNCA, $^1H_i-^{15}N_i-^{13}C\alpha_i$ correlated 3D NMR; HN(CO)CA, $^1H_i-^{15}N_i-^{13}C\alpha_{i-1}$ correlated 3D NMR; ssDNA, single-stranded deoxyribonucleic acid; H-bond, hydrogen bond; RMSD, root mean square deviation; SA, simulated annealing.

S0006-2960(95)02656-0 CCC: $12.00

contributes ~70% of the free energy of binding to ssDNA (Kumar et al., 1990a). The domain confers processivity to DNA synthesis in a short DNA gap (Singhal & Wilson, 1993), is required for full DNA polymerase activity (Kumar et al., 1990a), and catalyzes excision of deoxyribose 5′-phosphate from ssDNA or from dsDNA containing a preincised abasic site (Matsumoto & Kim, 1995).

The NMR assignments of ^{1}H, ^{15}N, and ^{13}C resonances and NOEs for the backbone and side chains (Liu et al., 1994) indicate that the N-terminal domain is an independently folded module consisting of four helices. Here we describe the three-dimensional structure of the N-terminal domain determined with high precision by multidimensional NMR under near-physiological conditions. Additionally, we mapped using NMR the interaction of this domain with ssDNA. An antiparallel helix-3−turn−helix-4 motif and residues adjacent to an Ω-type loop connecting helices 1 and 2 form the ssDNA interaction surface. The solution structure and the mapped effects reveal the first structural information on a ssDNA template interaction for a DNA polymerase.

EXPERIMENTAL PROCEDURES

Sample Preparation. The N-terminal fragment of rat DNA polymerase β (residues 2−87 with sequence ^{2}SKRKAPQE-^{10}TLNGGITDML-^{20}VELANFEKNV-^{30}SQAIHKYNAY-^{40}RKAASVIAKY-^{50}PHKIKSGAEA-^{60}KKLPGVGTKI-^{70}AEKIDEFLAT-^{80}GKLRKLEK; Kumar et al., 1990b) was overexpressed in the *Escherichia coli* strain BL21 (DE3)/pLysS harboring the expression plasmid pRSET-8k. The ^{15}N- or ^{15}N/^{13}C-enriched fragment was purified as described previously (Prasad et al., 1993; Liu et al., 1994). The purified protein domain was exchanged into 5 mM Tris-d_{11}, pH 7.5, and 400 or 100 mM NaCl by elution from a Sephadex G15 column. All buffers and salt solutions were passed over Chelex-100 resin (Bio-Rad) before use. The N-terminal domain was concentrated using a Centricon-3 (Amicon), and the pH was adjusted to 6.7. Two samples for homonuclear 2D NMR experiments contained 1.4 mM nonlabeled N-terminal domain. Two samples for ^{15}N-correlated 2D and 3D NMR experiments contained 4.7−5.0 mM ^{15}N-labeled N-terminal domain. A sample for 3D triple resonance and 3D ^{13}C-edited TOCSY and NOESY contained 2.8 mM ^{15}N/^{13}C-labeled N-terminal domain. A sample for p(dT)$_8$ binding studies contained 1.2 mM ^{15}N-labeled N-terminal domain after addition of p(dT)$_8$. The p(dT)$_8$ was purchased from GENOSYS. The p(dT)$_8$ was freed from contaminating buffers by elution from a G15 column prewashed with 50 mM EDTA and equilibrated with 50 mM $NH_4(HCO_3)$. The $NH_4(HCO_3)$ was removed by lyophilization. The p(dT)$_8$ was dissolved as a stock solution (19.4 mM) in 5 mM Tris-d_{11} and 100 mM NaCl, and the pH was adjusted to 6.7.

NMR Structure Determination. The NMR structure determination used previously described methodology (Kline et al., 1988). A set of 55 refined structural conformers was calculated using 1030 experimental NOE distance restraints, 52 ϕ and 16 χ_1, χ_2 torsion angle restraints, and 22 hydrogen bond restraints for amides within the interior of helices (Table 1). Data were collected at 27 °C using a highly modified GE GN500 NMR spectrometer (Liu et al., 1994). The following NMR experiments were performed for resonance assignments (Liu et al., 1994) and for structure determination: 2D NOESY (Jeener et al., 1979; Kumar et al., 1980), 2D DQF-COSY (Rance et al., 1983), 3D ^{1}H−^{15}N NOESY−HMQC (Kay et al., 1989), 3D ^{1}H−^{15}N TOCSY−HMQC (Kay et al., 1989), 3D ^{1}H−^{13}C NOESY−HMQC (Ikura et al., 1990), 3D ^{1}H−^{13}C TOCSY−HMQC (Liu et al., 1994), 2D ^{1}H−^{15}N HMQC (Bax et al., 1983), 2D ^{1}H−^{15}N HMQC-*J* (Kay & Bax, 1990), 3D HNCA (Kay et al., 1990), and 3D HN(CO)CA (Ikura & Bax, 1991). Other than HMQC-*J*, experiments that were performed in 90% H_2O/10% D_2O utilized DANTE water presaturation for 0.5 s of a 1 s relaxation delay prior to implementation of the first 90° pulse in the sequence. The HMQC-*J* data were acquired with DANTE presaturation during the entire 1 s relaxation delay. The ^{1}H−^{15}N NOESY−HMQC data were collected at mixing times of 100 and 200 ms. ^{1}H−^{13}C NOESY−HMQC data were collected at mixing times of 200 and 300 ms. All other acquisition parameters were as described previously (Liu et al., 1994).

NOE Distance Restraints. Patterns of helical NOEs were identified in the N-terminal domain (Liu et al., 1994). The interproton distances for the $d_{NN(i-i+2)}$, $d_{\alpha N(i-i+2)}$, $d_{\alpha N(i-i+3)}$, $d_{\alpha N(i-i+4)}$, and $d_{\alpha\beta(i-i+3)}$ NOEs within helices were classified into the range of 1.8−5.0 Å (Wüthrich, 1986). Calibration of $d_{NN(i-i+2)}$, $d_{\alpha N(i-i+2)}$, $d_{\alpha N(i-i+2)}$, $d_{\alpha N(i-i+3)}$, $d_{\alpha N(i-i+4)}$, and $d_{\alpha\beta(i-i+3)}$ NOEs in helices to the 1.8−5.0 Å distance classification is based on the interproton distances predicted for helices (Wüthrich, 1986). Three conservative upper bounds limits of ≤2.7 Å (strong), ≤4.0 Å (medium), and ≤5.0 Å (weak) (Wüthrich, 1986, 1989; Clore & Gronenborn, 1993) were evaluated for NOEs in 2D NOESY, 3D ^{1}H−^{15}N NOESY−HMQC, and ^{1}H−^{13}C NOESY−HMQC spectra at a mixing time of 200 ms. The upper bounds were evaluated from the NOE intensities relative to the calibrated NOE intensities within a particular spectrum using methods described previously (Wüthrich, 1986, 1989) and the procedures described below. NOE intensities were evaluated from the number of contours using Felix 2.10 software (BioSym Technologies). The contour levels were displayed using a factor of 1.2 or 1.4 times the preceding contour level. As has been recently described by Folmer et al. (1995), NOE intensities in 3D ^{15}N- or ^{13}C-edited NOESY−HMQC spectra can be influenced not only by the interproton distance but also by the efficiency of magnetization transfer to the heteronucleus and the relaxation rate ($1/T_2$) of the heteronucleus. Corrections relative to intensities of the ^{1}H−^{15}N HMQC spectrum or the ^{1}H−^{13}C HMQC spectrum, while in principle feasible, in practice would not be applicable in the presence of overlaps or window functions that enhance the separation of cross peaks. In the 2D ^{1}H−^{15}N HMQC spectrum, several cross peaks displayed lower intensities. Considerable differences in intensities were observed for a proton pair in the ^{13}C-edited NOESY depending on the attached ^{13}C nucleus in the ^{1}H−^{13}C transfer. To compensate for intensity variations in 3D NOESY spectra, the majority of NOE intensities assigned in the 3D ^{15}N-edited NOESY were classified into an interproton distance restraint range of 1.8−4.0 or 1.8−5.0 Å, while essentially all NOEs assigned in the 3D ^{13}C-edited NOESY (if not classified on the basis of 2D NOESY) were classified into a restraint range of 1.8−4.0 or 1.8−5.0 Å. The intensities of weak NOEs assigned at 300 ms were evaluated at 200 and 100 ms.

Classification of NOEs into Interproton Distance Ranges. The interproton distances for d_{NN} NOEs, which were more

Table 1: Structural Statistics[a]

statistics	⟨SA⟩	$\overline{(SA)}_r$
RMSD with respect to $\overline{(SA)}_r$		
helices (15−26, 36−47, 56−61, 69−78)		
heavy backbone atoms	0.64 ± 0.15	
all heavy atoms	1.10 ± 0.13	
residues 14−81		
heavy backbone atoms	1.24 ± 0.24	
all heavy atoms	1.71 ± 0.23	
RMSD (Å) for experimental restraints[b]		
all distance restraints (1074)	0.023 ± 0.002	0.024
interresidue sequential ($\|i-j\|=1$) (238)	0.026 ± 0.003	0.029
interresidue medium range ($1<\|i-j\|\le 5$) (175)	0.030 ± 0.006	0.028
interresidue long range ($\|i-j\|>5$) (152)	0.096 ± 0.010	0.100
intraresidue (465)	0.002 ± 0.000	0.000
hydrogen bonds[c] (22)	0.026 ± 0.004	0.030
torsion angles[d] (68)	0.489 ± 0.123	0.551
F_{NOE} (kcal·mol^{-1})[e]	28.9 ± 4.6	30.9
F_{tor} (kcal·mol^{-1})[e]	1.05 ± 0.53	1.11
F_{repel} (kcal·mol^{-1}) [f]	76.9 ± 8.8	64.3
$E_{L\text{-}J}$ (kcal·mol^{-1})[g]	−149.6 ± 28.3	−155.8
$E_{L\text{-}J}$ (kcal·mol^{-1})[h]	−95.6 ± 11.7	−91.8
RMSD from idealized covalent geometry[i]		
bonds (Å)	0.004 ± 0.000	0.004
angles (deg)	0.591 ± 0.024	0.551
impropers (deg)	0.418 ± 0.043	0.434

[a] The notation ⟨SA⟩ (Nilges et al., 1988) represents the 55 structures determined by molecular dynamics/simulated annealing using energy terms for NOE distance restraints, torsion angle restraints, bonds, angles, impropers, and hard sphere van der Waals contacts. The notation $\overline{(SA)}_r$ represents the structure determined by restrained minimization of the mean structure obtained by calculation of the average coordinates of the ⟨SA⟩ structures. The RMSD from the experimental restraints are with respect to the upper and lower limits of the distance or torsion angle restraints. [b] The number of each class of experimental restraints is given in parentheses. No distance restraints are violated by distances greater than 0.5 Å. [c] Backbone H-bonds employed restraints of 1.7−2.3 Å for the amide NH to carbonyl oxygen distance and 2.7−3.3 Å for the amide nitrogen to carbonyl oxygen distance. [d] Torsion angle restraints consisted of 52 ϕ and 16 χ_1 and χ_2 restraints. No torsion angles are violated by values greater than 5°. [e] The force constants used for the potential energy terms were 50 kcal·mol^{-1}·Å^{-2} for F_{NOE} and 200 kcal·mol^{-1}·rad^{-2} for F_{tor}. [f] The hard sphere van der Waals repulsion term F_{repel} was calculated with a force constant of 4 kcal·mol^{-1}·Å^{-2} with the van der Waals radii set to 0.8 times the values used in the CHARMM-19 parameters. [g] The Lennard-Jones 6−12 energy calculated within QUANTA using the CHARMM-19 parameters. [h] The Lennard-Jones 6−12 energy calculated within InsightII. [i] The impropers maintain planarity and chirality.

intense than the $d_{NN(i-i+2)}$, $d_{\alpha N(i-i+2)}$, $d_{\alpha N(i-i+3)}$, and $d_{\alpha N}(i_{-i+4})$ NOEs, were classified as 1.8−4.0 Å. The interproton distances for weak d_{NN} NOEs were classified as 1.8−5.0 Å (Wüthrich, 1986). There were no interproton distances for d_{NN} NOEs classified as 1.8−2.7 Å. The interproton distances for $d_{\beta N}$ and other sequential NOEs were classified into one of the three distance ranges on the basis of intensities relative to the weak $d_{NN(i-i+2)}$, $d_{\alpha N(i-i+2)}$, $d_{\alpha N(i-i+3)}$, and $d_{\alpha N(i-i+4)}$ NOEs. As predicted for helices the $d_{\alpha N(i-i+1)}$ NOEs were found to be of weak intensity. Interproton distances for 141 of 153 long-range NOEs were classified as 1.8−5.0 Å, interproton distances for 9 long-range NOEs stronger than calibrated $d_{\alpha\beta(i-i+3)}$ NOEs were classified as 1.8−4.0 Å, and interproton distances for 3 long-range NOEs identified in 2D NOESY in D_2O were classified as 1.8−2.7 Å. A total of 31 (the majority intraresidue) of 1030 NOEs were classified into a distance range of 1.8−2.7 Å. For NOEs with intensities bordering between the medium−strong or medium−weak classifications, the weaker distance range was used, thereby reducing errors due to indirect NOE contributions (Driscoll et al., 1989). Classification of the restraints as primarily 1.8−4.0 or 1.8−5.0 Å eliminated errors in NOE distance restraints that result from restraints being too tight due to the effects described in the previous section. As shown here, a high precision structure determination is obtained from a large number of restraints per residue classified as medium (1.8−4.0 Å) and weak (1.8−5.0 Å). Very strong NOEs were observed for the amide side chain protons of Asn and Gln in 2D NOESY and ^{15}N-correlated 3D NOESY spectra. Strong NOEs were observed for the geminal $\alpha\alpha'$ protons of Gly in the peptide backbone and the $\delta\delta'$ protons of Pro in 2D NOESY and ^{13}C-correlated 3D NOESY spectra.

For NOEs arising from methyl protons, aromatic ring protons, and non-stereospecifically assigned methylene protons, upper limit distance restraints were corrected for center averaging (Wüthrich et al., 1983). For distances involving methyl groups, 0.5 Å was added to the upper bound limit to account for the higher intensity. Only intraresidue NOEs that restrain (or potentially restrain) side chain conformations were included. As further detailed in the experimental section on χ_1 torsion angles, NOEs that included the intraresidue NOEs were useful in the determination of χ_1 torsion angle restraints, consistent with $J_{\alpha\beta}$ couplings in a set of 33 preliminary structures. Distance restraints for NOEs between geminal protons were not introduced into the structure calculation. Intraresidue NOEs that may not determine a unique side chain conformation were not determined and would not adversely affect the structure determination.

Data Analysis for H-Bond Restraints. A total of 22 H-bonds, each constrained by two distance restraints (Driscoll et al., 1989), were included as $r_{O(i)-N(j)} \le 3.3$ Å and $r_{O(i)-NH(j)} \le 2.3$ Å for $i-j$ residues as follows: helix-1 (15−19, 16−20, 17−21, 18−22, 19−23, 20−24, 21−25), helix-2 (37−41, 38−42, 39−43, 40−44, 41−45, 42−46, 43−47), helix-3 (57−61, 58−62), and helix-4 (69−73, 70−74, 71−75, 72−76, 73−77, 74−78). In the SA approach, H-bonds (and electrostatic interactions) were not implicitly introduced into the structure by the force field used in the calculations. Each

of the above described H-bonds were within well-defined α-helices and were included at positions in which the carbonyl-acceptor oxygen could be evaluated. No H-bonds were included for residues *i* through *i*+3 at the N-termini of helices, where *i* represents the amino-terminal residue in the helix. As described for the helical domain of resolvase (Liu et al., 1994), we found that slow NH exchange data at the N-termini of helices (based on deuterium exchange) could not be evaluated *a priori* in terms of H-bond acceptors, because capping residues or 3_{10} helix formation at the N-termini of helices is not readily determinable by a nonstructural analysis of NOE patterns.

For the N-terminal domain of β-Pol, H-bonds were assessed as being in an α-helix from the following data: (1) an absence of saturation transfer from the water resonance to the amide proton at pH 6.7 (i.e., exchange rates $<\sim 1\ s^{-1}$) as determined from comparison of hard presaturation versus jump-and-return methods of water suppression in collecting $^1H-^{15}N$ HMQC spectra (Bax et al., 1990); (2) observation of d_{NN}, $d_{NN(i-i+2)}$, $d_{\alpha N(i-i+2)}$, $d_{\alpha N(i-i+3)}$, $d_{\alpha(i-i+4)}$, and $d_{\alpha\beta(i-i+3)}$ NOEs; (3) measured or estimated $J_{NH\alpha}$ coupling constants of <6 Hz for all H-bonded residues (except K61 and L62); and (4) $^{13}C_\alpha$ chemical shifts indicative of helix (Spera & Bax, 1991) for all H-bonded residues (Liu et al., 1994). For extended segments, amide proton resonance intensity for several residues was substantially reduced or eliminated by 1 s water presaturation.

Deuterium Exchange Experiments. To further determine the exchange lifetime of the amide protons in the N-terminal domain, a deuterium exchange experiment was performed. Using a sample of the nonlabeled N-terminal domain in 5 mM Tris-d_{11}, pH 6.7, and 400 mM NaCl, repeated dilution with D_2O was followed by concentration in a Centricon-3. Low-intensity amide protons were observed along the diagonal of a 100 ms NOESY spectrum recorded within 24 h of initiating exchange; however, cross peaks were not observed that could allow assignments. The H51 amide resonance overlapped with that of the nonexchangeable H51 C4H. In a second experiment, a 90% H_2O/10% D_2O sample of the N-terminal domain in a solution containing 5 mM Tris-d_{11}, pH 6.7, and 400 mM NaCl was lyophilized and redissolved in an equal volume of D_2O. A $^1H-^{15}N$ HMQC spectrum showed that the amide protons in the domain predominantly exchanged with deuterons within minutes of dissolution of the lyophilized powder. Rapid exchange after lyophilization suggests unfolding on dehydration. We have also found that partial unfolding of the N-terminal domain occurs at temperatures above 35 °C and at pH <4.7 (Liu et al., 1994).

φ Torsion Angle Restraints. The φ torsion angle restraints were determined by analysis of the HMQC-*J* spectrum (Kay & Bax, 1990) and direct measurement of the $J_{NH\alpha}$ couplings in the ^{15}N dimension (Liu et al., 1994). $J_{NH\alpha}$ couplings of <6 Hz, corresponding to φ angles of $-60° \pm 30°$, were measured or estimated for residues within helix-1 (15−25), helix-2 (36−47), helix-3 (58−60), and helix-4 (69−78) and for residues 6, 8, 11, 28, 30, 33, 49, and 52.

$J_{NH\alpha}$ couplings of >8 Hz corresponding to φ angles of $-120° \pm 40°$ were observed for K48 at the C-terminus of helix-2, N12 at the N-terminus of helix-1, T79 and K81 at the C-terminus of helix-4, and V65 within the reverse turn.

Data Analysis for the φ Torsion Angle Restraints for K61 and L62. Residues 61 and 62 at the C-terminus of helix-3 displayed $J_{NH\alpha}$ couplings of 7.3 Hz, and NOEs indicate only a helical conformation for residues 61 and 62. Weak $d_{\alpha N(i-i+3)}$ NOEs were observed between E58 and K61 and between A59 and L62. Medium intensity d_{NN} NOEs and weak $d_{\beta N}$ NOEs were observed between K60 and K61 and between K61 and L62. A weak $d_{NN(i-i+2)}$ was observed between A59 and K61. A weak $d_{\alpha N(i-i+2)}$ NOE was observed between K60 and L62. Weak $d_{\alpha N}$ NOEs were observed between K60 and K61 and between K61 and L62. The $J_{NH\alpha}$ couplings for K61 and L62 and the NOE data were only consistent with a restraint range of $-80° \pm 30°$. The $d_{\alpha N}$ NOEs were weak and did not indicate averaging.

χ1 Torsion Angle Restraints. The χ_1 torsion angles and stereospecific assignments (Supporting Information, Table 1) were determined by analysis of the $J_{\alpha\beta}$ couplings measured from a DQF-COSY spectrum processed with a resolution of 1.47 Hz/point and from NOESY data acquired at a mixing time of 100 ms. Singular ranges of χ_1 torsion angles for F25, Y36, Y39, and Y49 were independently determined from the NOE data in 33 preliminary X-PLOR structures lacking χ_1 torsion angle restraints and analyzed using the program NMR Structure Determination within QUANTA 4.0 (Molecular Simulations). Aromatic side chains of F25, Y36, Y39, Y49, and F76 displayed preferred rotomeric conformations about χ_1 as determined from an analysis of the active and passive couplings for resolved $H\alpha-H\beta^2$ and $H\alpha-H\beta^3$ cross peaks. $J_{\alpha\beta}$ couplings of ≥ 10 Hz were observed for I15, I33, I46, I69, and I73 and for V20, V29, and V65, corresponding to a range of $-60° \pm 50°$ and $180° \pm 50°$, respectively, for the χ_1 torsion angles for these two groups of residues. A $J_{\alpha\beta}$ coupling of 8 Hz was observed for V45, and the χ_1 torsion angle was assigned as $60° \pm 50°$ on the basis of the 33 NOE-determined structures. The χ_1, χ_2 torsion angles and stereospecific assignments of the δCH_3 resonances for L62 and L19 were determined from the 33 NOE-determined structures and the $J_{\alpha\beta}$ and $J_{\beta\gamma}$ couplings.

SA Calculations of the Structure. Calculations of the NMR structure utilized the program X-PLOR (version 3.1, Brünger, 1992) on a Silicon Graphics Challenge. An extended starting structure was folded using the *ab initio* simulated annealing protocol within X-PLOR (Nilges et al., 1988; Brünger, 1992) by heating to 3000 K for 21 000 high-temperature steps followed by 14 000 cooling steps. The hard sphere van der Waals radii were set to 0.75 times (repel = 0.75), the value in the CHARMM-19 parameter set (parallhdg.pro). Force constants used for the potential energy terms in the calculations are described in the legend for Table 1. Of the 125 independently calculated structures, 60 displayed no NOE violations >0.3 Å, no dihedral angle violations $>3°$, and energies of less than 130 kcal/mol. These structures were refined by heating to 1000 K followed by 5000 cooling steps. The van der Waals radii in these structures were set to 0.8 times the CHARMM-19 van der Waals radii. Of these 60 refined structures, 55 displayed no NOE violations >0.5 Å or dihedral angle violations $>5°$.

NMR of the N-Terminal Domain−p(dT)8 Complex. $^1H-^{15}N$ HMQC data were acquired using a GE GN500 NMR spectrometer. Concentrations at the end of the $p(dT)_8$ titration were 1.2 mM for the N-terminal domain and 1.9 mM for $p(dT)_8$ in a solution of 5 mM Tris-d_{11}, pH 6.7, and 100 mM NaCl. After the 1D titration, the following spectra were recorded using parameters described previously (Liu et al., 1994): a $^1H-^{15}N$ HMQC spectrum, a 3D ^{15}N-edited

NOESY spectrum at a 200 ms mixing time, 2D NOESY spectra in 90% H_2O/10% D_2O at 200 and 300 ms mixing times, and a 3D ^{15}N-edited TOCSY spectrum. At this stage, a 1:1 binding stoichiometry was confirmed by quantitative recovery of excess $p(dT)_8$ from the protein−DNA complex after successive dilution of the 600 μL sample (with three 150 μL and two 225 μL aliquots of buffer) and centrifugal ultrafiltration using a 3 kDa cutoff filter (Centricon-3) to concentrate the sample to 600 μL. Recovered $p(dT)_8$ was quantified by measuring UV absorptivity ($\epsilon_{266} = 8660$ M^{-1} cm^{-1}; Cassani & Bollum, 1969). The concentration of $p(dT)_8$ in the sample after the first 150 μL dilution and reconcentration to 600 μL was 1.6 mM $p(dT)_8$ on the basis of the amount of $p(dT)_8$ recovered and the initial concentration of $p(dT)_8$ (1.9 mM). The concentration of $p(dT)_8$ in the sample after the subsequent dilutions that totaled 750 μL (see above) and reconcentration was 1.3 mM $p(dT)_8$ on the basis of the additional amount of $p(dT)_8$ recovered. A ^{1}H−^{15}N HMQC spectrum was recorded after removal of excess $p(dT)_8$. At this stage, the domain−DNA complex (1.2 mM) was titrated with a 4 M stock NaCl solution, and ^{1}H−^{15}N HMQC spectra were recorded. The sample was diluted with 5 mM Tris-d_{11} to a NaCl concentration of 100 mM and subsequently concentrated using a Centricon-3. A ^{1}H−^{15}N HMQC-*J* spectrum was recorded on the 1:1 complex of N-terminal domain−$p(dT)_8$ at a concentration of approximately 1 mM.

Analysis of ssDNA Binding to the N-Terminal Domain by 1D NMR Titration. A titration curve for $p(dT)_8$ binding was obtained by measuring the chemical shift change of the nondegenerate amide proton resonance of L77 in a 1D ^{1}H NMR titration of the N-terminal domain. The initial concentration of the N-terminal domain was 1.4 mM, and the final concentration after the titration was 1.2 mM. The average concentration used to fit the titration curve was 1.28 mM. The dissociation constant was fit using eq 1, which was derived from eq 2. In eqs 1 and 2, δ_{av} is the observed

$$\delta_{av} - \delta_F = x(\delta_B - \delta_F) \quad (1)$$

$$\delta_{av} = x\delta_B + (1 - x)\delta_F \quad (2)$$

(average) chemical shift at each titration point, δ_F is the chemical shift of the protein domain in the absence of ssDNA, and δ_B is the chemical shift of the protein domain when fully bound by ssDNA. The mole fraction (x) of the protein domain bound with ssDNA is defined by eq 3, in

$$x = [P_B]/[P_T] \quad (3)$$

which $[P_B]$ is the concentration of the protein domain bound, and $[P_T]$ is the total concentration of the protein domain. The mole fraction used to fit the titration curve was calculated for the total substrate concentration at each point in the titration and from the fitted dissociation constant using eqs 3 and 4. In eq 4, K_D is the dissociation constant, $[S_T]$ is the

$$[P_B] = \{(K_D + [S_T] + [P_T]) - [(K_D + [S_T] + [P_T])^2 - 4[S_T][P_T]]^{1/2}\}/2 \quad (4)$$

total concentration of ssDNA at each titration point, and $[P_T]$ and $[P_B]$ are as defined above. The value of $\delta_B - \delta_F$ used in the best fit was 0.161. A 1:1 stoichiometry for binding was determined from the break in the titration curve.

Analysis of the NaCl Dependence of ssDNA Binding to the N-Terminal Domain. The salt dependence of the association constant (K_A) of the N-terminal domain−$p(dT)_8$ complex was evaluated using the method described by Record et al. (1976). A log K_A vs log [Na] plot was constructed from ^{1}H chemical shift changes for N37, E71, K72, and E75. The K_A at each NaCl concentration was determined from the percentage of free and bound N-terminal domain on the basis of the average value of the chemical shift. At 100 mM NaCl, δ_B of the complex was set equal to δ_{av}, consistent with the finding that at this NaCl concentration only excess $p(dT)_8$ was isolated from the complexes (as described above). The mole fraction of bound N-terminal domain was evaluated at 200, 300, and 400 mM NaCl using eq 1. The association constant (K_A) was calculated from the mole fraction of bound N-terminal domain and eqs 5−7,

$$K_A = [P_B]/[P_F][S_F] \quad (5)$$

$$[P_T] = [P_B] + [P_F] \quad (6)$$

$$[S_T] = [P_B] + [S_F] \quad (7)$$

where $[P_F]$ is the free N-terminal domain concentration, $[S_F]$ is the free $p(dT)_8$ concentration, and the other terms are as described above.

RESULTS

Analysis of the NMR Structure. Nearly complete assignments of the ^{1}H, ^{15}N, and ^{13}C resonances of the backbone and side chains have been reported previously (Liu et al., 1994). In solving the tertiary packing, multiple iterative rounds of preliminary structural calculations were performed, initially using sequential, medium-range, and unambiguous long-range NOEs, followed by further analysis of long-range NOEs, stereospecific assignments, and determination of χ_1 and χ_2 torsion angles. Long-range NOEs were assigned in the 2D NOESY, ^{15}N-edited 3D NOESY, and ^{13}C-edited 3D NOESY spectra. NOEs arising from aliphatic side chain−side chain contacts between the helices were assigned in the ^{13}C-edited 3D NOESY spectrum. Of the 1030 NOE distance restraints used in the calculation, 999 restraints are medium (1.8−4.0 Å) and weak (1.8−5.0 Å). The precision of the structure determination results from the large number of approximate interproton distance and dihedral angle restraints per residue, as has been previously described by Clore and Gronenborn (1993). For residues 12−81 of the domain, this structure calculation utilized *14 restraints per residue*, not including H-bond restraints.

The 55 SA structures displayed no violations of NOEs >0.5 Å or dihedral angle violations of >5° and an average of 0.56 NOE violations >0.3 Å and 0.45 dihedral angle violations >3°. The RMSD for backbone atoms of helices with respect to their average position was 0.64 Å. For all heavy atoms within helices the RMSD was 1.10 Å (Table 1). The RMSD for backbone atoms within residues 14−81 was determined to be twice as large as for the helices (1.24 Å) and, as will be described, was due to the K27−K35 segment connecting helices 1 and 2 and the segment K52−S55. The 55 structures (Figure 1A) displayed small RMSD for distance restraints, torsion angle restraints, and covalent geometry (Table 1). The structure calculation utilized hard sphere van der Waals repulsive terms. The negative Len-

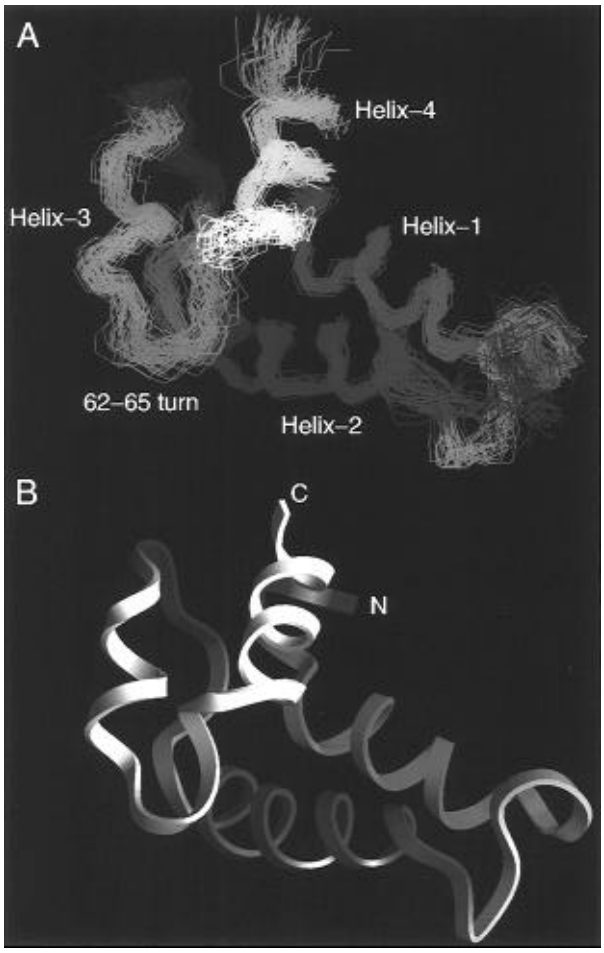

FIGURE 1: NMR structure of the N-terminal domain of rat DNA polymerase β. (A) The backbone trace of 55 SA conformers superimposed on the mean coordinate position for these structures with respect to the four helices: helix-1 (14−26) in green, helix-2 (33−48) in red, helix-3 (56−62) in magenta, and helix-4 (68−78) in yellow. Residues 27−32 are in an open conformation in 30 of the 55 SA structures and are displayed in orange. The 62−65 turn is depicted in gray for residues 63−65, and the 48−51 turn is shown in light blue for residues 49−51. Residue 48 is shared between helix-2 and the 48−51 turn. Residue 62 is shared between helix-3 and the 62−65 turn. (B) A ribbon representation of the minimized average structure (residues 10−78). All color figures were displayed using InsightII, BioSym Technologies, Inc.

nard-Jones energies in these structures independently confirmed the quality of the structures and that the NOE restraints resulted in packing with favorable contacts.

Description of the Structure. The N-terminal domain consists of antiparallel pairs of helices, with helix-1 (15−26)/helix-2 (36−47) crossing at an angle of +25° and helix-3 (56−61)/helix-4 (69−78) crossing at a angle of −20° (Figure 1). The pairs of helices interact with an overall crossing angle of approximately 50°. Helix-4 lies across the long axes of the predominantly hydrophobic face of helix-1 (crossing at −50°) and the hydrophobic face of helix-2 (crossing at −55°). The remainder of the domain consists of two turns (48−51 and 62−65), an Ω-type loop (27−35) and extended structure. The Ω-loop structure in proteins was initially described by Leszczynski and Rose (1986), and the functional significance of the Ω-loop structure has recently been reviewed (Fetrow, 1995). The pairs of helices pack with a V-like shape, with helix-4 and the K27−K35 flexible loop forming the sides of a somewhat depressed molecular surface. A slight bend is detectable along the

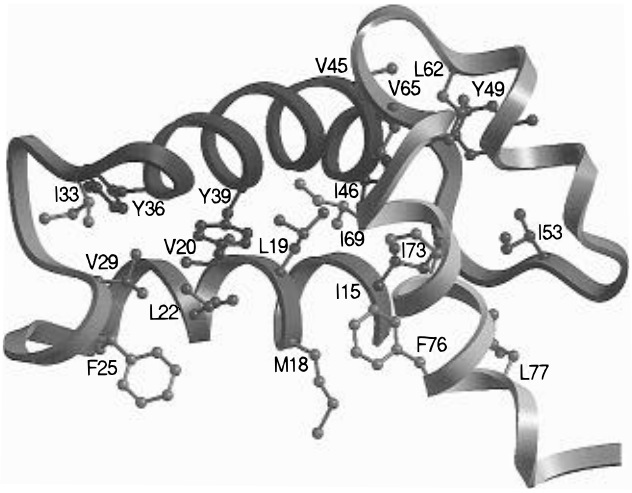

FIGURE 2: Hydrophobic side chains in the minimized average structure of the N-terminal domain of β-Pol. Branched side chains that are buried and hydrophobic are colored identically to the colored ribbon segments of secondary structure. The solvent-exposed hydrophobic side chains of M18, F25, I33, and V45 are colored light blue.

length of helix-2 (Figure 2) and is found in all calculated structures (Figure 1). Hydrophobic residues within the interior of the protein domain are contributed by each of the helices and turns (Figure 2). Of the five aromatic residues, Y39, Y49, and F76 are well buried and are hydrophobically conserved between β-Pol and the terminal deoxynucleotidyltransferase. The aromatic ring of F25 is exposed and is not conserved (Figure 3). The N-terminus of helix-1 and the C-terminus of helix-4 are near each other. A flexible amino-terminal arm (residues 2−10) extends away from the N-terminus of helix-1.

Turns and Loops. Turns are found between adjacent helices in the structure. The turn within residues 62−65 (Figure 1) displays a determined CO(i)-NH(i+3) H-bond with a distance of 2.2 Å in the minimized average structure. The 62−65 H-bond was not entered as a restraint. The turn within residues 48−51 displays an unusual interaction in which the amide proton of H51 (very slow exchange of >3 days) is in the face of the Y49 aromatic ring but not hydrogen-bonded to the K48 carbonyl oxygen. Similarly, no H-bond restraint was used for the amide proton of H51. The upfield shift of this amide resonance (6.32 ppm) (Liu et al., 1994) and the slow exchange indicated a type of "H-bond" with the aromatic π-cloud. Amino−aromatic interactions have been previously described for an SH2 domain (Waksman et al., 1993). Residues 52−54 are in an extended conformation alongside helix-3 and show broad downfield-shifted amide proton resonances (8.98, 9.37, 9.14 ppm). The K27−K35 Ω-type loop connecting helix-1 and helix-2 displays multiple conformations in the SA structures (Figure 1A). Each of the determined conformations is consistent with the NOE data within the loop, but preferred or multiple conformations in solution are not determinable from the interproton NOEs alone. A complete study of the backbone dynamics of the N-terminal domain using approaches described previously (Farrow et al., 1994) is in progress and will be presented elsewhere.

Binding of p(dT)$_8$ to the N-Terminal Domain: 1D NMR Titration. In studying the effects of p(dT)$_8$ binding, the N-terminal domain was titrated with a 19.4 mM stock solution of p(dT)$_8$. 1D NMR spectra in 90% H_2O/10% D_2O

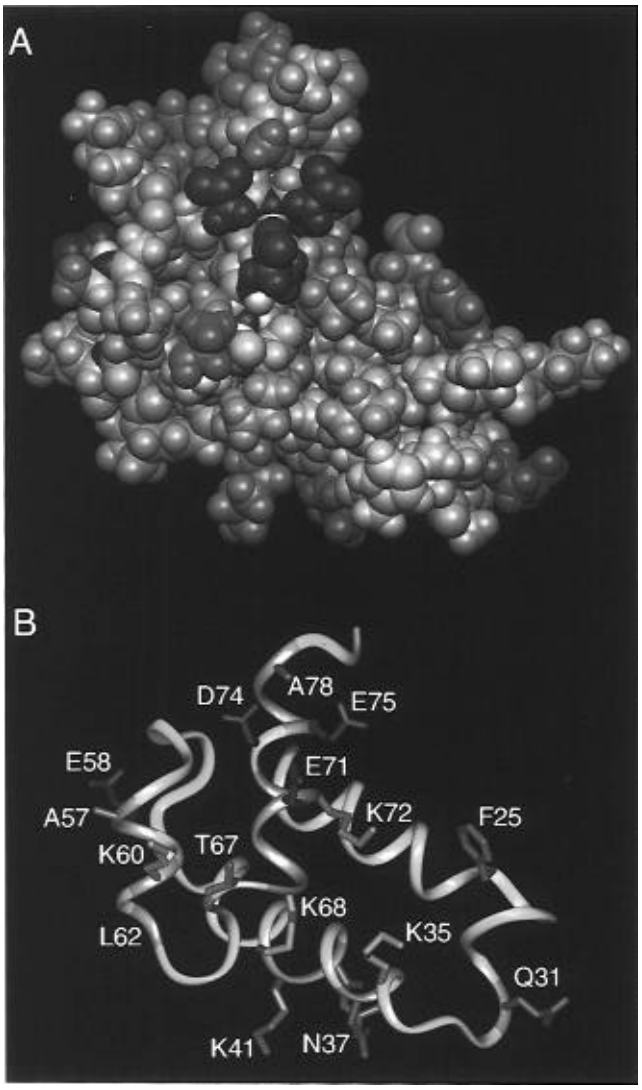

FIGURE 3: Space-filling (A) and stick (B) representations of the N-terminal domain of DNA polymerase β. Illustrated in gray on the yellow ribbon are chemical shift changes determined for Q31, N37, R40, K41, A47, A57, E58, K60, L62, G66, K68, I69, A70, E71, K72, I73, E75, F76, L77, and A78. The chemical shift changes for L82 and R83 in the unstructured segment are not shown. The mapped chemical shift changes are $\geq$0.1 ppm for ^{1}H or $\geq$0.4 ppm for ^{15}N. Intermolecular NOEs to p(dT)$_8$ were assigned for T67, A57, and F25 (see Figure 10). Side chains of residues displaying the NMR-determined chemical shift changes and NOEs are shown in light blue (positively charged), red (negatively charged), green (hydrophilic), orange (exposed hydrophobic), and magenta (buried hydrophobic). The D74 side chain, which together with E71 and E75 forms the three-carboxylate site, is also shown in red, although the chemical shift changes for this residue (more remote from E71 and K72) are less. Exposed amide NH groups for residues displaying chemical shift changes are shown in the space-filling representation in deep blue (nitrogens) and white (protons) (A). Side chains of the affected buried hydrophobics (A47, L62, I69, A70, I73, F76, and L77) are not shown in (B). The side chain of K35 which contributes charge to the binding surface near K72 is shown in light blue. The cross peak for K35 was too weak to detect in the complex.

were collected at each titration point. The amide proton resonance of L77 was observed to shift downfield during the titration. The change in the chemical shift of the L77 resonance is interpreted as resulting from the chemical shifts for the free (δ_F) and the bound forms (δ_B) of the L77 resonance being averaged into a single resonance (δ_{av}) [i.e., $(\delta_F - \delta_B) \ll k_{off}$ for the complex; Raftery et al., 1968]. Fitting of the titration curve for the amide proton resonance of L77

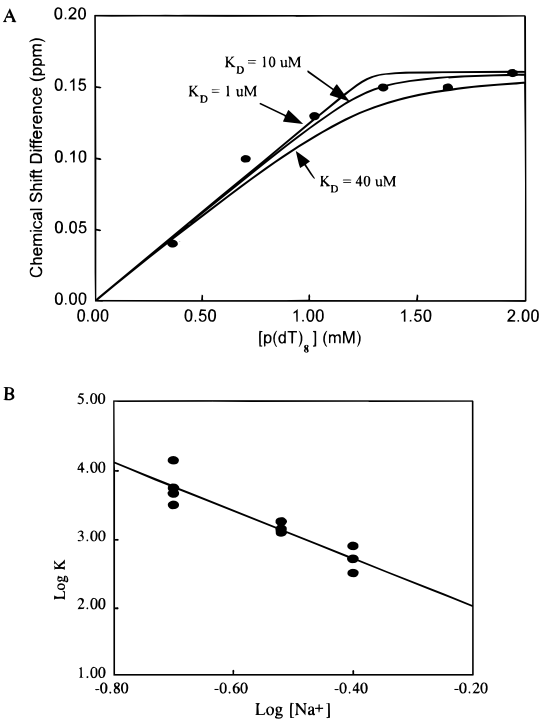

FIGURE 4: Determination of the dissociation constant for p(dT)$_8$ binding to the N-terminal domain of β-Pol and the contribution of ionic effects to binding. (A) 1D NMR titration measuring the chemical shift change for the nondegenerate L77 amide proton on addition of p(dT)$_8$. A best fit K_D of 10 μM is shown. (B) A log K_A vs log [Na] plot in which the ^{1}H chemical shift changes for N37, E71, K72, and E75 were measured as a function of NaCl concentration and used to determine the mole fraction of p(dT)$_8$-bound N-terminal domain. The determined slope is -3.5, and the extrapolated K_A at 100 mM NaCl corresponds to a K_D of 15 μM.

indicates that the N-terminal domain binds p(dT)$_8$ as a 1:1 complex with a K_D of 10 μM in 100 mM NaCl (Figure 4A). This measurement is within error limits of the dissociation constant ($K_D = 15$ μM) determined from the salt dependence of the association constant (Figure 4B) using data from ^{1}H$-^{15}$N HMQC spectra at 100, 200, 300, and 400 mM NaCl (Figure 5) as described in the next section. The 1D titration method was only useful for the non-overlapping L77 resonance.

Binding of p(dT)$_8$ to the N-Terminal Domain: NaCl Titration and Effects on ^{1}H and ^{15}N Chemical Shifts. Before removal of excess p(dT)$_8$, 2D NOESY, ^{1}H$-^{15}$N HMQC, ^{15}N-edited 3D NOESY$-$HMQC, and ^{15}N-edited 3D TOCSY$-$HMQC spectra were recorded. After removal of excess p(dT)$_8$, ^{1}H$-^{15}$N HMQC spectra were recorded for the N-terminal domain$-$p(dT)$_8$ complex at NaCl concentrations of 100, 200, 300, and 400 mM NaCl. An overlay of the ^{1}H$-^{15}$N cross peaks from the salt titration (Figure 5) illustrates that increasing NaCl concentrations resulted in a shift of the cross peaks toward the chemical shifts of the free state of the domain. Control experiments showed that the chemical shifts of the N-terminal domain alone were unaffected by NaCl concentrations of 100$-$400 mM. The cross peaks for N37, E71, K72, and E75 were sufficiently resolved during the titration to allow determination of the mole fraction of protein bound with p(dT)$_8$ at each salt concentration. The NaCl titration method for analysis of the K_A (i.e., $1/K_D$) differed from the above-described p(dT)$_8$ titration in that the concentration of p(dT)$_8$ was not changed. A log K_A vs log [Na] plot (Figure 4B) yielded a slope of

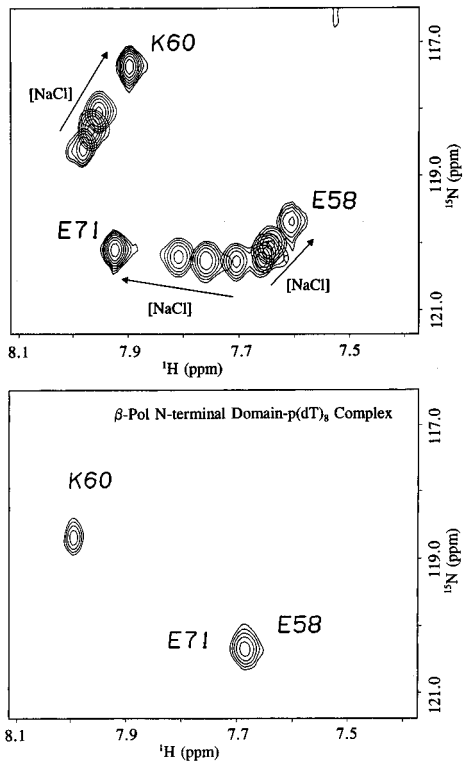

FIGURE 5: A region of the overlaid ^{1}H−^{15}N HMQC spectra of the N-terminal domain in the absence and presence of p(dT)$_8$ at increasing NaCl concentrations. (Top) The directions of the arrows represent the change in the position of the cross peaks under the following conditions: N-terminal domain−p(dT)$_8$ at 100 mM NaCl after removal of excess p(dT)$_8$, the complex at 200 mM NaCl, the complex at 300 mM NaCl, and the N-terminal domain alone at 400 mM NaCl. (Bottom) The N-terminal domain−p(dT)$_8$ complex in the presence of excess p(dT)$_8$ showing the ^{1}H−^{15}N correlations for K60 and E71/E58 (superimposed under these conditions).

−3.5 ± 0.5, indicative of ionic contacts in the complex (Record et al., 1976). Extrapolation to 100 mM NaCl yielded a determined dissociation constant of 15 μM, which was within experimental error limits of that determined from the 1D NMR titration (Figure 4A).

The 2D ^{1}H−^{15}N HMQC spectra at each salt concentration were used together with the 3D ^{1}H−^{15}N-edited NOESY and the 2D NOESY spectra of the complex in making assignments of backbone ^{1}H and ^{15}N resonances in the N-terminal domain−p(dT)$_8$ complex. Of the 79 amides in residues 5−86 of the domain, 75 were assigned in the p(dT)$_8$ complex (Table 2, Supporting Information). Except as noted below, ^{1}H and ^{15}N chemical shifts and $J_{NH\alpha}$ couplings were measured in the HMQC-*J* spectra recorded for the 1:1 complex of the N-terminal domain and p(dT)$_8$ (Figure 6A) and for the N-terminal domain alone (Figure 6B). Chemical shifts for K5, A6, L11, G13, G14, K35, and T67 were measured in ^{1}H−^{15}N HMQC spectra with p(dT)$_8$ in excess. Chemical shift changes of ≥0.1 for ^{1}H and ≥0.5 for ^{15}N were determined for Q31, R40, K41, A47, A57, E58, K60, L62, G66, I69, A70, E71, K72, I73, E75, F76, L77, A78, L82, and R83 (Figure 7). In addition, changes of −0.09 ppm in the ^{1}H chemical shift and −0.4 ppm in the ^{15}N chemical shift were measured for N37, and a change of 0.4 ppm was measured in the ^{15}N chemical shift of K68. A change of −0.4 ppm was measured in the ^{15}N chemical shift of L85.

The T67 amide ^{1}H and ^{15}N resonances were assigned in the complex on the basis of weak d_{NN} and medium $d_{\alpha N}$ connectivities in 2D NOESY spectra of the complex. A weak cross peak was observed in the HMQC experiment with a 0.5 s water presaturation time (^{1}H 9.51, ^{15}N 115.3) (Figure 8). The T67 amide proton resonance was not observed for the N-terminal domain alone (due to rapid NH

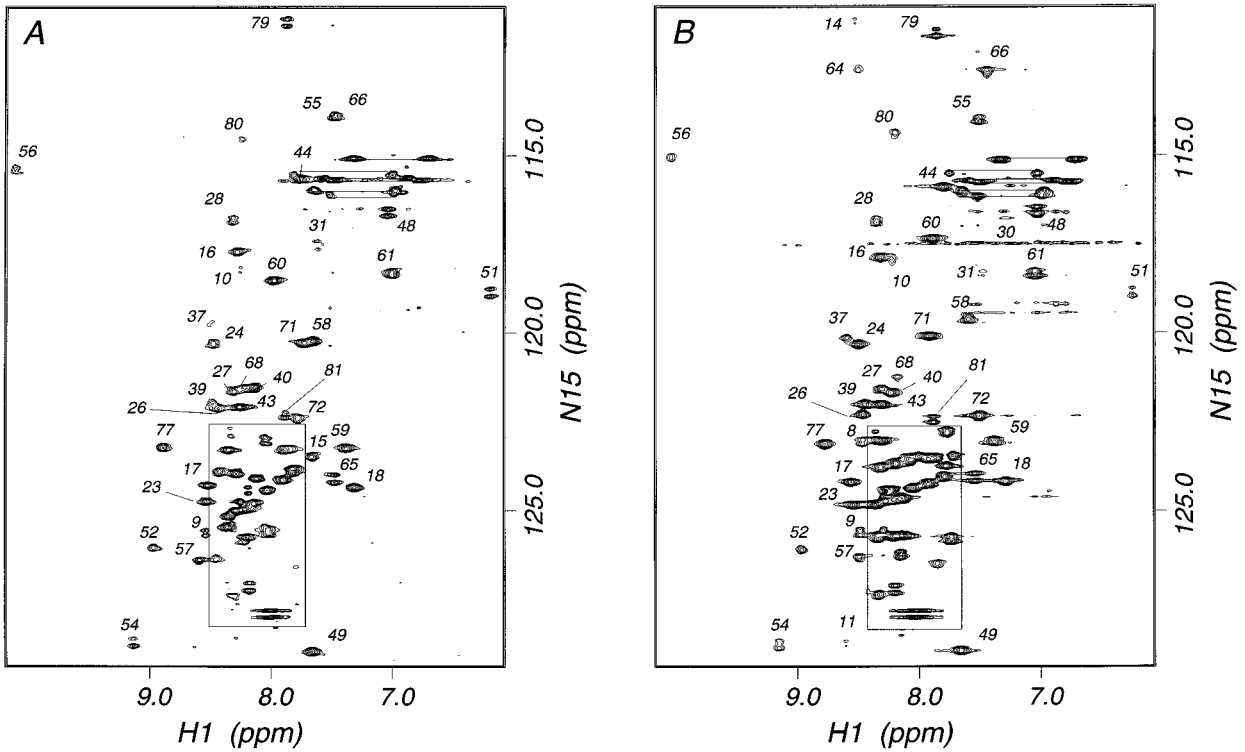

FIGURE 6: HMQC-*J* spectra in which $J_{NH\alpha}$ couplings were allowed to evolve during t_1. Comparative spectra of the N-terminal domain−p(dT)$_8$ complex (A) and the N-terminal domain alone (B). The spectra were acquired with a 1 s water presaturation time. Both spectra were processed using method 2 (Kay & Bax, 1990), with exponential line broadening of 15 Hz in t_2 and a squared sine bell shifted by 30° in t_1. The F_1 resolution is 1.22 Hz/point. All cross peaks have been assigned, and those within the boxed region are shown in Figure 9C, D.

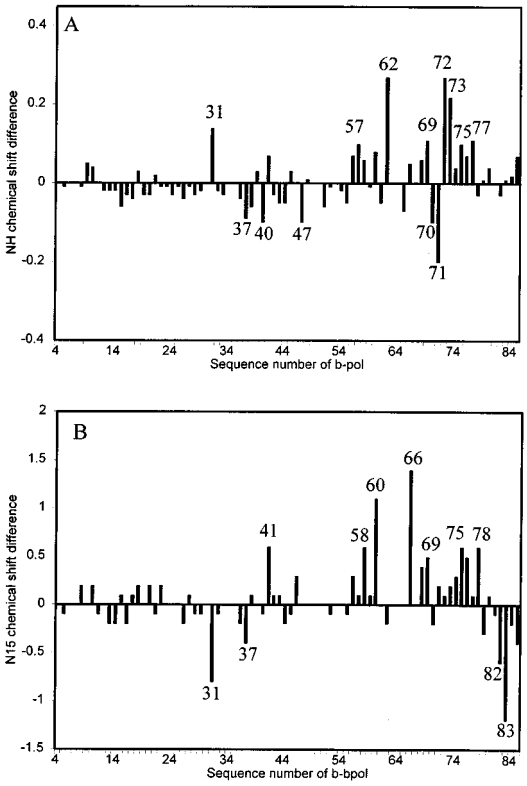

FIGURE 7: Chemical shift changes for the N-terminal domain on complex formation with $p(dT)_8$. The chemical shift differences (domain complex−domain free) for the amide proton chemical shifts (A). The chemical shift differences for the amide ^{15}N chemical shifts (B). In (B) K68, F76, and L85 show significant changes of 0.4, 0.5, and −0.4 ppm and are not annotated due to crowding in the figure.

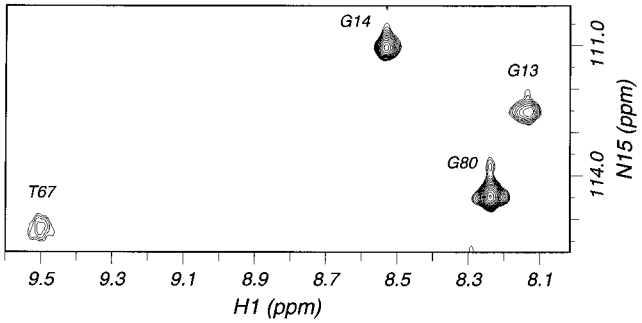

FIGURE 8: Expanded region of the $^1H-^{15}N$ HMQC spectrum of the N-terminal domain−$p(dT)_8$ complex, showing the cross peaks for G13, G14, T67, and G80. These residues do not display H-bonds in the structure. The cross peaks are observed with a 0.5 s water presaturation time at pH 6.7 and are reduced or eliminated by a 1 s presaturation time (Figure 6). G64 is not observed in the complex.

exchange or possibly to conformational exchange broadening). Cross peaks for G13 and G14 (Figure 8) as well as for K5, A6, and L11 were observed in the HMQC spectrum of the complex (and the N-terminal domain alone). Cross peaks for K5, A6, L11, G13, and G14 are weak or missing in the HMQC-*J* spectra. No assignments were made for S30, K35, and G64 in the complex. $^1H-^{15}N$ cross peaks for S30, K35, and G64 are non-overlapping in $^1H-^{15}N$ HMQC spectra of the N-terminal domain alone, but the intensities are weak. The weak cross peaks for S30, K35, and G64 were not observed in the $p(dT)_8$ complex or on addition of NaCl to the complex. The H34 amide resonance was unassigned for the complex and for the N-terminal domain alone.

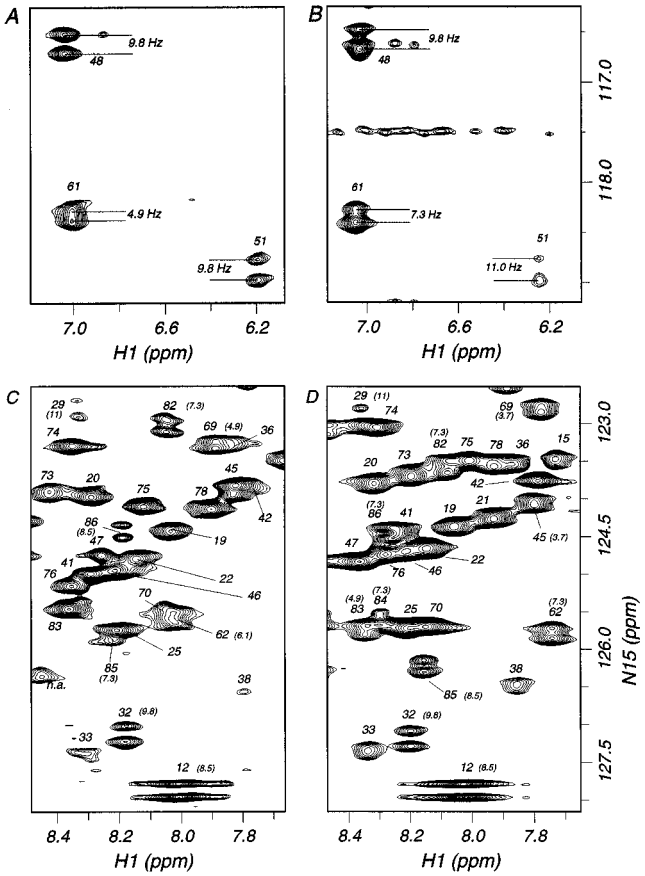

FIGURE 9: Expanded regions of the HMQC-*J* spectra of the N-terminal domain−$p(dT)_8$ complex (A and C) and the N-terminal domain alone (B and D), showing changes in chemical shifts and the overall similarity in $J_{NH\alpha}$ coupling constants. The spectra were processed as described in the legend to Figure 6. All cross peaks have been assigned except that designated n.a. (not assigned) in (C); this resonance likely results from K3, R4, or K87.

Binding of $p(dT)_8$ to the N-Terminal Domain: Measurement of $J_{NH\alpha}$ Coupling Constants. The $J_{NH\alpha}$ couplings were evaluated from $^1H-^{15}N$ HMQC-J spectra recorded for the N-terminal domain−$p(dT)_8$ complex and the N-terminal domain alone (Figures 6 and 9). The coupling constants were measured from the splitting between the data points at the peak and were accurate to ±1.2 Hz. As described by Kay and Bax (1990), the measured $J_{NH\alpha}$ coupling constants in the ^{15}N dimension of the HMQC-*J* spectra were affected by the line width such that, for $J_{measured} > 8$ Hz, $J_{correct} \leq J_{measured}$, and for $J_{measured} < 5$ Hz, $J_{correct} \geq J_{measured}$. The corrections factors for the previous two cases are 1−2 Hz depending on the line width as described by Kay and Bax (1990). For $J_{measured}$ values of 5−8 Hz, less than 1 Hz corrections are necessary (Kay & Bax, 1990). For T10, N12, V29, A32, K48, H51, K54, V65, T79, K81, K82, L85, and E86, the $J_{NH\alpha}$ coupling constants were measured (all ≥7.3 Hz) and were not affected by $p(dT)_8$ binding within the accuracy of the measurement (Figures 6 and 9). The $J_{NH\alpha}$ coupling for K61 was measured as 4.9 Hz in the $p(dT)_8$ complex and as 7.3 Hz in the absence of $p(dT)_8$ (Figure 9A,B). The $J_{NH\alpha}$ coupling for I69 was measured as 4.9 Hz in the $p(dT)_8$ complex and 3.7 Hz in the absence of $p(dT)_8$ (Figure 9C,D). The $J_{NH\alpha}$ coupling for N28 was measured as 7.3 Hz in the $p(dT)_8$ complex and 6.1 Hz in the absence of $p(dT)_8$ (Figure 6). The $J_{NH\alpha}$ coupling for T10 was measured as 6.1 Hz in the $p(dT)_8$ complex and 4.9 Hz in the

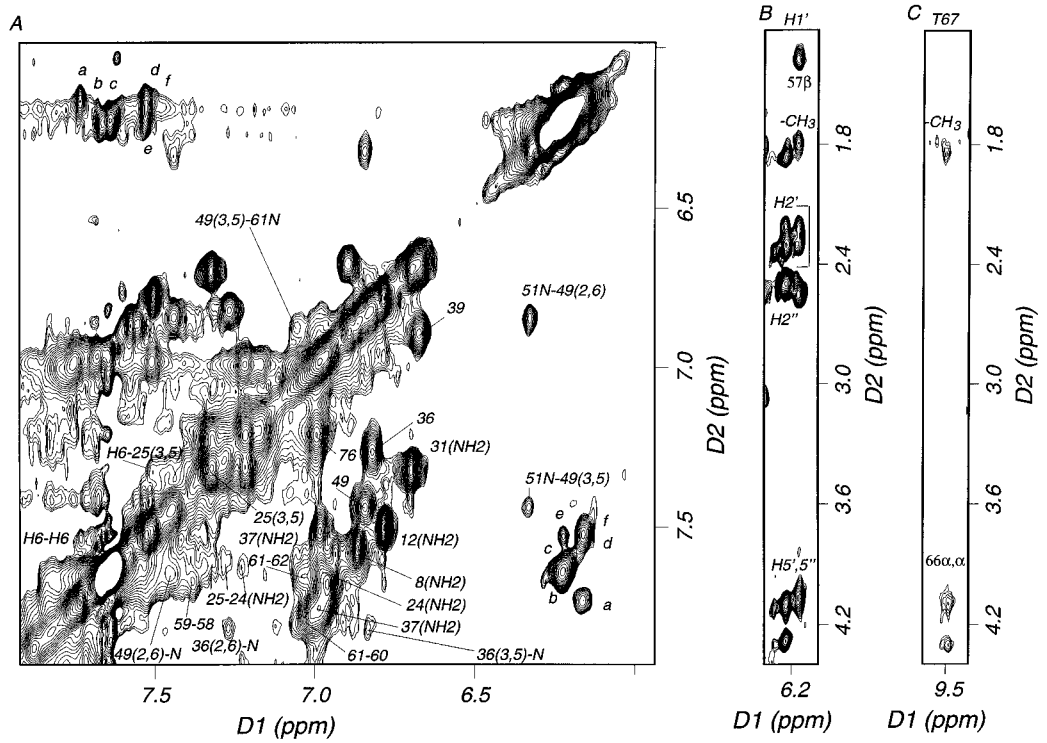

FIGURE 10: Expanded regions of the 300 ms NOESY spectrum of the N-terminal domain−p(dT)$_8$ complex with the N-terminal domain at 1.2 mM and p(dT)$_8$ at 1.9 mM in 90% H_2O/10% D_2O containing 5 mM Tris-d_{11}, pH 6.7, and 100 mM NaCl at 27 °C. The spectrum was processed with a squared sine bell window function shifted by 90° and a 2 Hz exponential multiplication in the t_1 and t_2 dimensions. Shown in (A) is the aromatic region with the intermolecular p(dT)$_8$ H6 to F25 C3,5H NOE. Cross peaks have been assigned by comparison to the NOESY spectrum of the N-terminal domain alone, by ^{15}N-edited 3D NOESY of the complex for amide protons, and by the NaCl titration for amide protons; the NOE correlations designated a−f are assigned to sequential and intranucleotide H1′−H6 interproton distances; the NOEs for side chain amide protons of Q8, N12, N24, Q31, and Q37 are designated by residue number; the NOEs for aromatic C2,6H to C3,5H protons of Y36, Y39, Y49, and F76 are designated by residue number; and the F25 C3,5H protons are at the diagonal among the adjacent upfield C4H and C2,6H protons of the F25 aromatic spin system. Shown in (B) is a strip along the H1′ resonances with the intermolecular NOE to the A57 β-methyl group; also shown are H1′ NOEs to H5′,5″ (internucleotide sequential), to H2′,2″ (intranucleotide), and to −CH_3 (internucleotide sequential); the groups of assigned H1′, H2″, H5′,5″, and H6 protons display altered chemical shifts vs those of p(dT)$_8$ alone and were assigned on the basis of the similarity to the chemical shifts for p(dT)$_8$ alone. The resonances for p(dT)$_8$ alone were assigned from TOCSY and NOESY data. Shown in (C) is a strip along the T67 amide proton resonance with an intermolecular NOE designated −CH_3 assigned to a methyl group of p(dT)$_8$; the $d_{\alpha N}$ NOEs from G66 are shown. A weak d_{NN} NOE from G66 was also observed (not shown).

absence of p(dT)$_8$ (Figure 6). Other $J_{NH\alpha}$ couplings, if not resolved, were estimated at <6 Hz. $J_{NH\alpha}$ coupling of >6 Hz were easily resolved for this domain, and $J_{NH\alpha}$ couplings of 3.7 Hz have been measured. Thus, we are assured that estimates of <6 Hz for those smaller than the line width are conservatively accurate.

Intramolecular p(dT)$_8$ NOEs. NOESY spectra of the N-terminal domain−p(dT)$_8$ complex were acquired at 200 and 300 ms mixing times. At a mixing time of 300 ms, the intensities of the intramolecular NOEs for p(dT)$_8$ in the complex (Figure 10) were considerably stronger than for p(dT)$_8$ alone (not shown). The NOEs in the complex provided independent confirmation of p(dT)$_8$ binding. The strengths of the NOEs were consistent with an increase in the effective correlation time for the dipolar interaction. We observed five strong H1′−H6 NOE correlations for p(dT)$_8$ on binding to the N-terminal domain (Figure 10A) as compared to two correlations for the p(dT)$_8$ alone (not shown). These H1′−H6 NOEs (Figure 10A) were characteristic of internucleotide sequential distances (3.5 Å in B-DNA) and intranucleotide H1′−H6 distances (4.0 Å). Each of the five correlations had H1′ and H6 chemical shifts differing from those for p(dT)$_8$ alone. Similarly, we observed five H1′−H2′ NOE correlations that were characteristic of intranucleotide interproton distances (2.9 ± 0.5 Å). We observed H1′−H5′, H5″ NOEs (Figure 10B) that were characteristic of internucleotide sequential interproton distances (3 Å in B-DNA) and three H1′−CH_3 NOEs (Figure 10B) that were characteristic of sequential interproton distances (∼4 Å). Cross peaks attributed to five nucleotides suggested that exchange (or sliding) between nucleotide-bound sites on the N-terminal domain was slow (with respect to the chemical shift difference). Several of the proton chemical shifts for sequential nucleotides were not averaged. The five H1′−H2′ cross peaks were consistent with nucleotides bound to the domain with each in a different chemical environment.

N-Terminal Domain−p(dT)$_8$ NOEs. The T67 amide proton showed a weak NOE to a proton with a resonance at 1.86 ppm consistent with an assignment to the most upfield of the two chemical shifts for the p(dT)$_8$ methyl protons (Figure 10C). The T67 amide proton is exposed at the surface of the domain (Figure 3A). The H1′ proton at 6.16 ppm showed a strong NOE cross peak to an alanine methyl resonance at 1.39 ppm (Figure 10B). Assignment of the H1′ NOE to the β-CH_3 protons of A57 was made after analysis of each of the βCH_3−NH cross peaks for the alanine residues. On the basis of H1′−H2′ NOEs, two nucleotides had an H1′ chemical shift of 6.16 ppm. The structure of the N-terminal domain suggests that separate nucleotides give

Chart 1

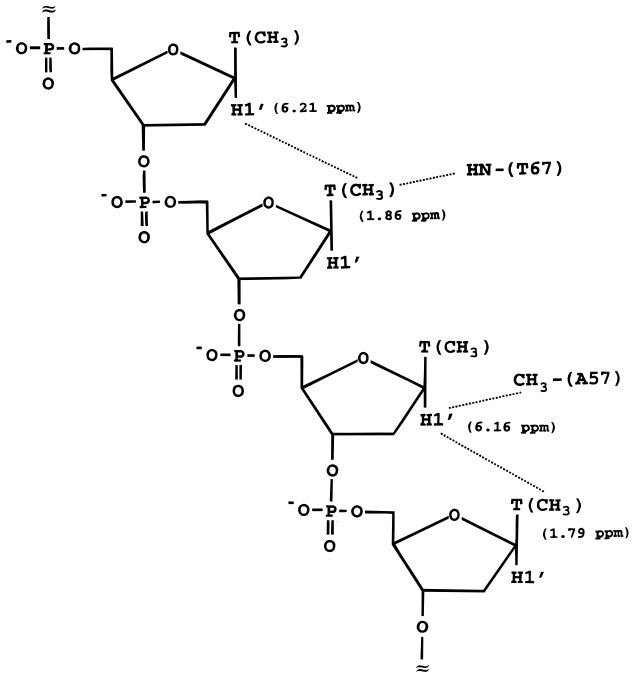

NOEs to T67 NH and A57 βCH_3 protons. The T67 NH and βCH_3 protons are ~11 Å apart. The following NOEs were consistent with the proximities shown in Chart 1: the sequential NOE between the H1′ proton at 6.21 ppm and the $p(dT)_8$ methyl protons at 1.86 ppm; the NOE between the $p(dT)_8$ methyl protons at 1.86 ppm and the T67 amide proton; and the NOE between the H1′ proton at 6.16 ppm and the A57 methyl protons. Assuming on the basis of the structure of the N-terminal domain that T67 and A57 contact sequential nucleotides, the NOE data in Figure 10 support a model with T67 in proximity to a nucleotide 5′ to the nucleotide in proximity to A57. An upfield H6 proton showed a weak NOE to the C3,5H protons of F25 (Figure 10A), and this cross peak was not present in the absence of $p(dT)_8$. The H6 proton showing the NOE to F25 showed only a weak H6−H1′ NOE (cross peak f) (Figure 10A).

A second possible set of NOEs from H6 to the F25 aromatic protons displayed overlap between the H6 and N24 side chain amide proton chemical shifts. The F25 aromatic protons gave weak NOEs to what was conservatively assigned to the side chain amide proton of N24 (Figure 10A). The other side chain amide proton showed overlap and therefore could not be used to confirm the N24−F25 NOEs (Figure 10A). The F25−N24 NOEs were not observed in the absence of $p(dT)_8$. One of the H6 proton chemical shifts overlapped with one of the N24 NH_2 chemical shifts. Thus, it is possible that a second H6 proton displays an NOE to the F25 aromatic protons, but the NOE could not be unambiguously assigned.

DISCUSSION

Mapping of the $p(dT)_8$ Interaction Interface. Residues displaying chemical shift changes and intermolecular NOEs on binding $p(dT)_8$ are illustrated in the solution structure of the N-terminal domain (Figure 3). Also highlighted are residues D74 and K35, which contribute to the surface charge potential surrounding residues implicated in binding. Surface residues displaying chemical shift changes are predominantly

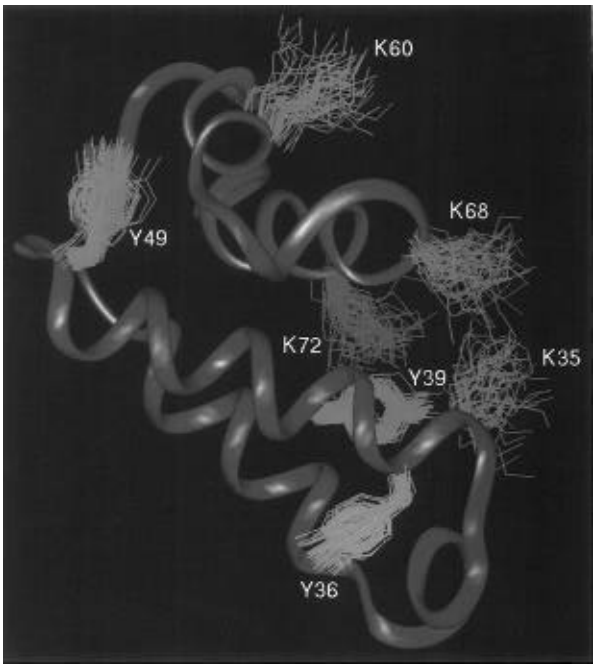

FIGURE 11: Ribbon representation of the average NMR structure of the N-terminal domain of β-Pol showing the flexibility in the 55 SA structures of the K35, K60, K68, and K72 side chains (in blue). Shown for comparison are the superimposed side chains of Y36, Y39, and Y49 (in yellow), which are more ordered in the 55 SA structures.

(although not entirely) clustered on one side of the domain. The exposed residues showing significant changes include Q31, N37, R40, K41, A57, E58, K60, G66, K68, E71, K72, E75, A78, L82, R83, and L85. Q31 is in the Ω-type loop. N37, R40, and K41 are adjacent to both the loop and helix-4. A57, E58, and K60 are in helix-3. G66 is between helices 3 and 4. E71, K72, E75, and A78 are in helix-4. L82, R83, and L85 are in the unstructured linker segment which in the full-length enzyme connects to the catalytic domain. Buried residues showing significant changes include A47, L62, I69, A70, I73, F76, and L77. A47 is in the helix-2 and packs with helix-1. L62 is in helix-3. I69, A70, I73, F76, and L77 are in helix-4. The chemical shift changes described above can be explained in terms of $p(dT)_8$ contacts and perturbation in the electrostatic charge distribution at the surface. For interaction at the N-terminus of helix-4, the effects on helix-4 chemical shifts may be propagated through the helix dipole. On the basis of the measurements of $J_{NH\alpha}$ coupling constants, no overall structural differences in the backbone ϕ angles are apparent on binding $p(dT)_8$. The chemical shift changes together with the limited number of intermolecular NOEs between the NH of T67 and a CH_3 of $p(dT)_8$ (weak), the CH_3 of A57 and an H1′ of $p(dT)_8$ (strong), and the C3,5H of F25 and an H6 of $p(dT)_8$ (weak) provide strong evidence that the binding surface is formed by residues on helix-3, residues at the N-terminus of helix-4, and the surface formed by helix-4 and the Ω-type loop (Figure 3).

Sites Appropriate for Nucleotide Contact on the Solution Structure. A potential site for phosphate contact is located at the H-bond donating groups that include the K35−ϵNH_3^+ and the K72−ϵNH_3^+ (Figure 3A). The edge of the aromatic ring of Y39 forms the bottom of a pocket between the K35 and K72 side chains (Figure 3A), and these three side chains are illustrated in Figure 11. Our assessment of the K72/K35 site is principally based on analysis of the structure (i.e.,

two positive charged residues), the chemical shift changes in helix-4, the large induced chemical shift change for K72 (possibly electrostatic), and the biochemical data for K72. We had previously suggested the K72/K35 site of interaction on the basis of the initial NMR results (Liu et al., 1994). A second potential site for phosphate contact is located at the hydrogen-bonding groups that include G64−NH, T67−γOH, T67−NH, and K68−ϵNH_3^+ (Figure 3A). At the second site, the phosphate could favorably interact with the positive helix dipole at the N-terminus of helix-4 and cap the exposed T67 amide proton. A third site for phosphate contact is possible at the ϵNH_3^+ group of K60 on helix-3. The K60 side chain is adjacent to the A57 methyl group to which an NOE has been assigned from H1′ of a nucleotide. Ionic contacts between the N-terminal domain and ssDNA are in agreement with the NaCl concentration dependence of the binding equilibrium. E71, D74, and E75 on helix-4 (Figure 3B) form a potential M^+ or M^{2+} binding site appropriate for cation-assisted phosphate contact adjacent to the K35/K72 site. Experiments are in progress to determine the effects of Mg^{2+} on complex formation. The aromatic side chain of F25 packs at the β-position as a singular χ_1 rotomer. A binding crevice for a base is associated with the exposed aromatic ring of F25 (Figure 3A); however, the weak F25 C3,5H NOEs to the base H6 protons (Figure 10A) suggest that the thymidine base does not fit well into the crevice. The remaining affinity of the domain for ssDNA in 300 mM NaCl at pH 6.7 suggests that hydrophobic contacts or possibly cation-assisted phosphate contact contributes to the binding.

Relationship of the Structure to ssDNA Binding and the DNA Polymerization Mechanism. The backbone conformations within the K27−K35 loop cluster into two approximate spatial conformations in the SA structures, which can be described as an open and closed form with respect to the adjacent helix-4 (Figure 1A). Helical conformations are observed for I33−N37. In the open form, the amide of Y36 is weakly hydrogen-bonded to the carbonyl oxygen of I33 in 30 of 55 structures [average Y36(NH)−I33(O) distance of 2.8 Å]. The role of the flexibility of the K27−K35 loop in phosphate contact at the K35/K72 site remains to be determined. The range of conformations for the side chains of K72, K68, and K60, and particularly for K35 at the Ω-type loop in the SA structures, is larger than those of the packed aromatic side chains (Y36, Y39, and Y49), as assessed from a comparison of the coordinates for the β and γ carbons for these side chains (Figure 11). Flexibility may be an important characteristic of the binding affinity for various single-stranded and abasic site-containing dsDNA substrates. The amino-terminal arm contains residues K3, R4, and K5 near the N-terminus, which are available to interact with the phosphate backbone of a larger gapped DNA duplex.

Common to all X-ray structures of DNA polymerases [reviewed by Arnold et al. (1995)] including the structure of the β-Pol catalytic domain ternary complex (Pelletier et al., 1994) has been the lack of contacts by the protein to ssDNA template at positions 5′ to the base-pairing dNTP site. In the crystallographic approaches, elements of the DNA polymerase structures and/or ssDNA templates necessary to observe the template interaction have either not been cocrystallized or have been crystallized and not observed in the electron density maps. For the Klenow fragment, a ssDNA interacted productively with the 3′−5′ exonuclease site (Beese & Steitz, 1991). DNA polymerase function in solution requires interaction with a flexible ssDNA template extending from the enzyme active site. DNA polymerases and HIV-1 reverse transcriptase are flexible proteins and display conformational changes in independently determined crystal structures of the same protein (Pelletier et al., 1994; Jäger et al., 1994). Flexibility is not typically observed in a single crystal packing environment. The interaction described here for β-Pol provides the first insight into a mechanism of ssDNA template binding with a DNA polymerase. The possible role of template strand binding in β-Pol catalysis is one of prevention of template misalignment on the 3′-primer.

Relationship of the Solution Structure to Single-Stranded DNA Binding, to Gapped 5′-Phosphate Binding, and to dRPase Activity. Binding studies and DNA polymerase activity measurements indicate that the N-terminal domain of β-Pol binds to ssDNA, increasing the polymerase activity of β-Pol (Kumar et al., 1990). The N-terminal domain also binds to a single-stranded five-nucleotide gap which contains a downstream 5′-phosphate (Singhal et al., 1993; Prasad et al., 1994). The N-terminal domain is required for full DNA polymerase activity (Kumar et al., 1990). Basu et al. (1989) performed DNA polymerase inhibition experiments using pyridoxal phosphate. The inhibitor pyridoxal phosphate was found to modify the side chain of K72 covalently. Protection against K72 modification by pyridoxal phosphate was afforded by the addition of template-primer and the complementary deoxynucleoside triphosphate substrates (Basu et al., 1989). K72 is exposed at the interaction surface mapped in the solution structure. Prasad et al. (1993) have shown that ssDNA cross-links to the N-terminal domain at residues S30 and H34. The NMR solution structure shows S30 and H34 to be in the Ω-type loop.

Matsumoto and Kim (1995) have shown that the N-terminal domain functions as a dRPase by removing deoxyribose 5′-phosphate from both dsDNA or from ssDNA. A deoxyribose 5′-phosphate (or nicked abasic site) is the product of uracil−DNA glycosylase catalyzed cleavage of a uracil base from a G-U mismatch followed by AP endonuclease cleavage of the abasic site [reviewed by Lindahl et al. (1979)]. Uracil−DNA glycosylase performs the first step in base excision repair from the G-U mismatch, and the human enzyme is highly conserved with the enzymes from bacteria, yeast, and viruses (Olsen et al., 1989). DNA polymerase β forms a complex with mammalian DNA ligase I (Prasad et al., 1996). Repair complexes with the N-terminal domain of DNA polymerase β, if such exist, would likely involve regions of the structure other than the mapped ssDNA binding face. Wilson et al. have found that mutation of K72 to alanine abolishes the dRPase activity of the N-terminal domain (unpublished). Thus, the active site for dRPase activity appears associated with helix-4, as does ssDNA binding. The ssDNA interaction surface of the N-terminal domain is of a length appropriate for binding a five-nucleotide single-stranded segment of a gapped DNA. We interpret the Mg^{2+} requirement, which was observed for the duplex but not the ssDNA dRPase activity (Matsumoto & Kim, 1995), as being a result of Mg^{2+} coordinating the carboxylates of E71, D74, and E75 and the phosphate backbone of the abasic site DNA. The details of how three different DNA substrates (i.e., ssDNA, gapped DNA, and nicked abasic site DNA) interact with the N-terminal domain remain to be determined. Further studies of nucleic acid

interaction with the N-terminal domain of β-Pol are in progress.

SUPPORTING INFORMATION AVAILABLE

A table of stereospecific assignments and χ torsion angles and a table of ^{1}H and ^{15}N chemical shifts for the N-terminal domain alone and in the complex with $p(dT)_8$ (3 pages). Ordering information is given on any current masthead page.

REFERENCES

Anderson, R. S.; Lawrence, C. B., Wilson, S. H., & Beattie, K. L. (1987) *Gene 60*, 163−173.

Basu, A., Kedar, P., Wilson, S. H., & Modak, M. J. (1989) *Biochemistry 28*, 6305−6309.

Bax, A., Griffey, R. H., & Hawkins, B. L. (1983) *J. Am. Chem. Soc. 105*, 7188−7190.

Bax, A., Ikura, M., Kay, L. E., Torchia, D. A., & Tschudin, R. (1990) *J. Magn. Reson. 86*, 304−318.

Beese, L. S., & Steitz, T. A. (1991) *EMBO J. 10*, 25−33.

Boosalis, M. S., Mosbaugh, D. W., Hamatake, R., Sugino, A., Kunkel, T. A., & Goodman, M. F. (1989) *J. Biol. Chem. 264*, 11360−11366.

Brünger, A. T. (1992) *X-PLOR Manual version 3.0*, Yale University, New Haven, CT.

Casas-Finet, J. R., Kumar, A., Morris, G., & Wilson, S. H. (1991) *J. Biol. Chem. 266*, 19618−19625.

Cassani, G. R., & Bollum, F. J. (1969) *Biochemistry 8*, 3928−3936.

Clore, G. M., & Gronenborn, A. M. (1993) in *NMR of Proteins* (Clore, G. M., & Gronenborn, A. M., Eds.) pp 1−27, CRC Press, Inc., Boca Raton, FL.

Driscoll, P. C., Gronenborn, A. M., Beress, L., & Clore, G. M. (1989) *Biochemistry 28*, 2188−2198.

Farrow, N. A., Muhandiram, R., Singer, A. U., Pascal, S. M., Kay, C. M., Gish, G., Shoelson, S. E., Pawson, T., Forman-Kay, J. D., & Kay, L. E. (1994) *Biochemistry 33*, 5984−6003.

Fetrow, J. S. (1995) *FASEB J. 9*, 708−717.

Folmer, R. H. A., Nilges, M., Konings, R. N. H., & Hilbers, C. W. (1995) *EMBO J. 14*, 4132−4142.

Fry, M., & Loeb, L. (1986) *Animal Cell DNA Polymerases*, CRC Press, Inc., Boca Raton, FL.

Ikura, M., & Bax, A. (1991) *J. Biomol. Nucl. Magn. Reson. 1*, 99−104.

Ikura, M., Kay, L. E., Tschudin, R., & Bax, A. (1990) *J. Magn. Reson. 86*, 204−209.

Jäger, J., Smerdon, S. J., Wang, J., Boisvert, D. C., & Steitz, T. A. (1994) *Structure 2*, 869−876.

Jeener, J., Meier, B. H., Bachmann, P., & Ernst, R. R. (1979) *J. Chem. Phys. 73*, 4546−4553.

Kay, L. E., & Bax, A. (1990) *J. Magn. Reson. 86*, 110−126.

Kay, L. E., Marion, D., & Bax, A. (1989) *J. Magn. Reson. 84*, 72−84.

Kay, L. E., Ikura, M., & Tschudin, R. (1990) *J. Magn. Reson. 89*, 496−514.

Kline, A. D., Braun, W., & Wüthrich, K. (1988) *J. Mol. Biol. 204*, 675−724.

Kumar, A., Ernst, R. R., & Wüthrich, K. (1980) *Biochem. Biophys. Res. Commun. 95*, 1−6.

Kumar, A., Abbotts, J., Karawya, E. M., & Wilson, S. H. (1990a) *Biochemistry 29*, 7156−7159.

Kumar, A., Widen, S. G., Williams, K. R., Kedar, P., Karpel, R. L., & Wilson, S. H. (1990b) *J. Biol. Chem. 265*, 2124−2131.

Kunkel, K. A. (1985) *J. Biol. Chem. 260*, 5787−5796.

Leszczynski, J. F., & Rose, G. D. (1986) *Science 234*, 849−855.

Lindahl, T. (1979) *Prog. Nucleic Acid Res. Mol. Biol. 22*, 135−192.

Liu, D.-J., DeRose, E. F., Prasad, R., Wilson, S. H., & Mullen, G. P. (1994) *Biochemistry 33*, 9537−9545.

Liu, T., DeRose, E. F., & Mullen, G. P. (1994) *Protein Sci. 3*, 1286−1295.

Matsumoto, Y., & Kim, K. (1995) *Science 269*, 699−702.

Mullen, G. P. (1995) *Methods Enzymol. 262*, 147−171.

Nilges, M., Gronenborn, A. M., Brünger, A. T., & Clore, G. M. (1988) *Protein Eng. 2*, 27−38.

Olsen, L. C., Aasland, R., Wittwer, C. U., Krokan, H. E., & Helland, D. E. (1989) *EMBO J. 8*, 3121−3125.

Pelletier, H., Sawaya, M. R., Kumar, A., Wilson, S. H., & Kraut, J. (1994) *Science 264*, 1891−1903.

Prasad, R., Kumar, A., Widen, S. G., Casas-Finet, J. R., & Wilson, S. H. (1993) *J. Biol. Chem. 268*, 22746−22755.

Prasad, R., Beard, W. A., & Wilson, S. H. (1994) *J. Biol. Chem. 269*, 18096−18101.

Prasad, R., Singhal, R. K., Srivastava, D. K., Molina, J. T., Tomkinson, A. E., & Wilson, S. H. (1996) *J. Biol. Chem.* (in press).

Raftery, M. A., Dahlquist, F. W., Chan, S. I., & Parsons, S. M. (1968) *J. Biol. Chem. 243*, 4175−4180.

Rance, M., Sorensen, O. W., Bodenhausen, G., Wagner, G., Ernst, R. R., & Wüthrich, K. (1983) *Biochem. Biophys. Res. Commun. 117*, 479−485.

Record, M. T., Jr., Lohman, T. M., & de Haseth, P. (1976) *J. Mol. Biol. 107*, 145−158.

Shibutani, S., Bodepudi, V., Johnson, F., & Grollman, A. P. (1993) *Biochemistry 32*, 4615−4621.

Singhal, R. K., & Wilson, S. H. (1993) *J. Biol. Chem. 268*, 15906−15911.

Singhal, R., Prasad, R., & Wilson, S. H. (1995) *J. Biol. Chem. 270*, 949−957.

Spera, S., & Bax, A. (1991) *J. Am. Chem. Soc. 113*, 5490−5492.

Waksman, G., Shoelson, S. E., Pant, N., Cowburn, D., & Kuriyan, J. (1993) *Cell 72*, 779−790.

Wüthrich, K. (1986) *NMR of Proteins and Nucleic Acids*, Wiley-Interscience, New York.

Wüthrich, K. (1989) *Science 243*, 45−50.

Wüthrich, K., Billeter, M., & Braun, W. (1983) *J. Mol. Biol. 169*, 949−961.

BI952656O